# Modelling of spatial distribution of segregations in large steel ingots by analysis of centimetric segregation maps

Lucie Gutman, J.R. Kennedy, Ahmed Kaci Boukellal, François Roch, Arthur Marceaux Dit Clément, Miha Založnik, J Zollinger

# Modelling of spatial distribution of segregations in large steel ingots by analysis of centimetric segregation maps



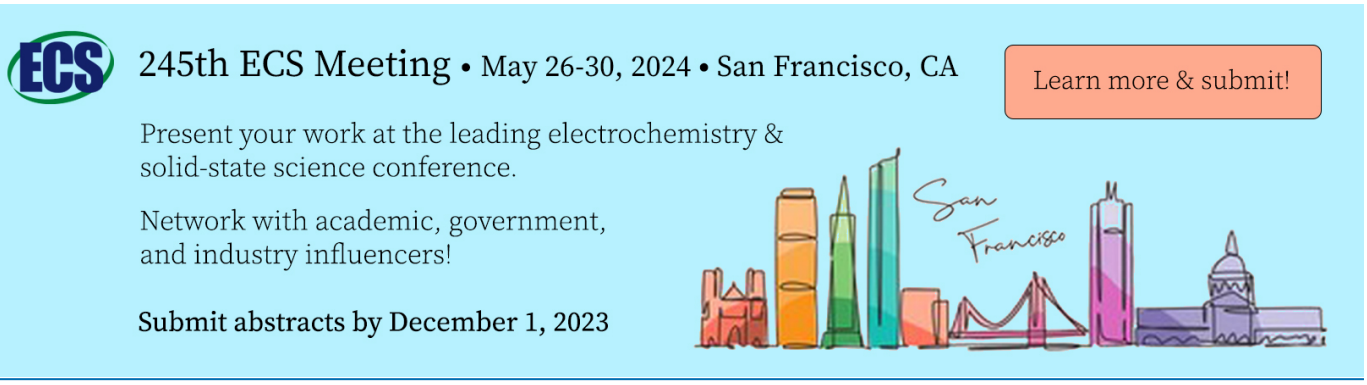

# Modelling of spatial distribution of segregations in large steel ingots by analysis of centimetric segregation maps

**L Gutman[1,2], J R Kennedy[2], A.K Boukellal, F Roch[1], A Marceaux dit Clément[1], M Založnik[2] and J Zollinger[2,*]**

[1] Framatome DTI, F-92400 Courbevoie, France
[2] Université de Lorraine, CNRS, IJL, F-54000 Nancy, France

* corresponding author: julien.zollinger@univ-lorraine.fr

**Abstract.** Mesosegregation appears during the solidification of low-alloyed steels at the scale of a few grains. It causes chemically segregated bands in forgings manufactured from steel ingots. As this may affect the mechanical properties of the produced parts, it is crucial to understand the formation of such segregation patterns. While both microsegregation and macrosegregation are well understood and can be readily characterized, little is known about the formation of mesosegregation. In this paper we present a data analysis method to identify the characteristic scales and patterns of mesosegregation. Segregation was mapped on centimetric samples, using micro X-Ray fluorescence (µXRF). The fine sampling grid used reveals segregation patterns at different scales. To identify and distinguish the mesoscale segregation patterns from smaller and larger present patterns, a numerical data analysis technique based on spatial filtering was used. It can identify characteristic scales of mesosegregation patterns on 2D serial cut samples, leading to 3D reconstruction. This approach combined with simulation studies, will ultimately pave the way to a comprehensive understanding of the formation of mesosegregation.

## 1. Introduction

Segregation is a very common phenomenon that occurs during alloy solidification. It consists in a local departure from the nominal concentration of the alloying elements in the liquid. It is positive when the local liquid is enriched, or negative when it is depleted. During steel solidification, the common alloying elements (for instance C, Mn or Mo) are rejected in the liquid phase [1]. Consequently, chemical heterogeneity appears in the solid phase at different scales. At the dendrite scale (from $\mu m$ to a few hundreds of $\mu m$), *microsegregation* is caused by the solute rejection into the liquid during the dendrite growth. It is generally affected by the partition coefficient $k$ at the solid-liquid interface and the solute diffusion in the two phases [2]. If the partition coefficient $k$ is smaller than 1 and diffusion is faster in the liquid, as with C, Mn and Mo in Fe, microsegregation creates depleted solid and enriched liquid. Such segregated phases move at the ingot scale ($m$) through convection, grain movement, solidification shrinkage and mushy zone deformation, leading to *macrosegregation* [3]. Heat treatment processes can reduce microsegregation through diffusion at the dendrite scale. Macrosegregation, however, cannot be reduced, as it is at a much larger scale. As a result, macrosegregation persists in the semi-products and even the final parts, thus affecting final mechanical properties [4].

Solid state transformations may be influenced by segregation, resulting in non-uniform microstructures associated with different local enrichments of the solid. Final mechanical properties are affected by microstructure, which can be related to certain segregation patterns. Hence segregation can affect the final mechanical properties. The shape, size and distribution of segregations are affected by the forging steps. Their intensity or number remain unchanged however [6]. During forging and hot

rolling certain segregation patterns are transformed (in shape and size) to banded patterns which can lead to anisotropic mechanical properties. In banded patterns, impact toughness is highly anisotropic: the measured toughness depends on the direction of sampling and its depth in the forged piece [7,8]. Hardness of the steel is linked to it carbon content; hence the hardness varies in banded segregations patterns, leading to hardness anisotropy in forged parts [9]. Residual stress in welds are also affected by banding since their distribution depends on phase transformation kinetics, hence chemical segregation [10]. Banding is caused by segregations at an intermediate scale between microsegregation (dendrite scale) and macrosegregation (ingot scale) [11]. Such intermediate scale segregations, probably at the grain-scale, are called *mesosegregations*. To control such banding phenomena, a thorough understanding of mesosegregation is key.

Understanding mesosegregation starts with comprehensive characterization of mesosegregated material. Different characterisation techniques have been developed to track chemical heterogeneities at different scales. Investigation of microsegregation is commonly carried out with an Electron Probe Micro Analyser (EPMA) which enables the quantification of the chemical composition with an interaction volume of roughly 1 $\mu m^3$ [9]. In large steel ingots, macrosegregation can be measured with Optical Emission Spectrometry (OES) or Infrared Combustion Analysis (ICA) for Carbon and Sulphur investigation. Macrosegregation can also be detected by X-Ray Fluorescence (XRF) spectroscopy [12]. Manganese (Mn) and Molybdenum (Mo) macrosegregation patterns can easily be distinguished, with a 5 mm analysis step and minimal sample preparation [13]. However, these techniques cannot be adapted to intermediate-scale segregation in the case of large ingots due to their spatial resolution being to large to resolve centimetric details. Solidification times in large ingots, such as those used in the nuclear industry, are very long (on the order of magnitude of ~10 ~100hours). As a result, investigated samples from these ingots present secondary dendrite arm spacing of 800 µm. To investigate the occurrence of mesosegregations in such ingots, chemical composition should be mapped at the centimetric, grain, scale. At this scale, none of the aforementioned techniques are suitable. On the fine scale, EPMA analysis is impractical: it provides more detail than necessary, is thus too time consuming, and it is non-trivial to analyze samples of the needed scale within conventional equipment. Conversely, the OES and ICA provide less details than needed due to their coarse, manual sampling methodology.

In this paper we analyzed the spatial distribution of segregation in a volume of 115 x 95 x 145 $mm^3$ based on a new sampling and characterisation methodology recently developed [14]. This new method, based on micro-X-Ray Fluorescence (µXRF), is promising for the chemical analysis of mesosegregation in steel ingots and enables the observation of channel segregates present within the sample volume. First, thirty chemical segregation maps were obtained using µXRF on serial cut samples. These maps were filtered to improve the detection of channel segregates. Then the filtered segregation maps were treated to detect intermediate scale segregation and channel segregates. Finally, these filtered and treated maps were used to reconstruct, in 3D, channel segregates and intermediate scales segregations present in the sample volume.

## 2. Material and methods

### *2.1. Samples*

The low-alloy steel 16MND5 (0.16 %wt. C, 1.45 %wt. Mn, 0.725 %wt. Ni and 0.5 %wt. Mo) was investigated. Samples were taken from the equiaxed region of a 116 t ingot.

As the aim of the study is to observe centimetric scale segregation volumetrically, centimetric scale sample plates were serial cut with a 5 mm step using wire electron discharge machining. The studied surfaces of the plates, the *x* and *y* directions, are perpendicular to the top of the ingot, while the *z* direction aligns with the height of the ingot and gravity. In total 30 plates were analyzed each with surface of 115 x 95 mm, *x* and *y*, and a distance of 5 mm, along the *z* direction, between each. In total a volume of 115 x 95 x 145 mm was analyzed. Samples are numbered successively from the bottom of the stack, N°1 being the lowest, closest to the bottom of the ingot, and N°30 being the highest, closest to the top of the ingot.

Several selected samples were etched with 3% Nital to reveal and characterize their solidification structure. On Nital etched surfaces, several structures overlap: both the solidified structure and solid-

state transformed structure can be observed. With repeated etching procedure, the solidification structure is highlighted, however primary austenitic grain boundaries are also visible as long bright lines crossing dendritic arms. The Nital etching procedure does not require a metallographic surface finish, samples were ground flat with MD discs (SiC abrasive in a resin matrix) to P1200 without diamond polishing. Figure 1 shows an example of the structures observed after such Nital etching.

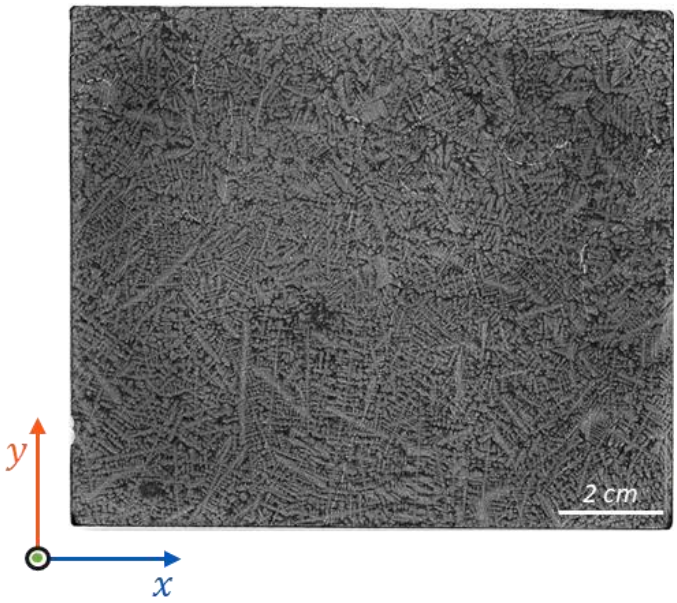


**Figure 1.** Optical macrograph of the lowest sample of the stack. Solid depleted in solute appears in light grey, while enriched regions appear in dark. The thin bright lines are primary austenitic grain boundaries.

*2.2. Micro-X-Ray Fluorescence (µXRF)*

A Bruker M4 Tornado device equipped with a Rh X-Ray source (30 W power) was used for Micro-X-Ray Fluorescence (µXRF) analysis. On both sides of the primary X-Ray source, there is an Energy Dispersive Spectroscopy detector. The samples were placed on a stage which moves dynamically below the fixed X-Ray source and detectors in a vacuum chamber (20 mbar vacuum). The spot size focused on the sample is 20 µm.

Optimization of the primary X-Ray sources conditions leads to a minimisation of artefacts and an improvement of the output signal. Several tests were performed to define the best conditions for the analysis of low alloyed centimetric-scale steel samples, with the objective to improve both Mn and Mo signals [13]. The best outcoming signal was obtained with an acceleration voltage of 50 keV, a 200 µA current and a 100 µm thick Al filter. The use of the filter allows analysis with a 20 % dead time (an indicator of minimized artefacts) without decreasing the current, and thus without weakening the output signal.

Once the X-Ray source conditions were selected, the acquisition time and analysis step size were defined. This choice is influenced by the size of the sample, the size of the structures desired to analyzed and the experimental time available. The sampling effect on centimetric scale samples has been investigated previously and the provided guidelines for sampling [13] were followed in the present work. A balance must be found between accuracy, obtained with an increase of analysis time and a decrease of analysis step, and reasonable experimental time. The analysis step set for all the samples investigated here was 100 µm, with an analysis time of 45 ms on each point. These settings enable the analysis of a single sample per night.

Comparison with EPMA measurement and between the different samples shows that the Mo-maps are more reliable than the Mn-maps. This can be explained by the proximity between the Mn peak and the iron (Fe) peak in the obtained XRF spectra. In low-alloyed steels, the Fe concentration is much higher than the concentration of any other element, and as such the Fe peaks are much larger than others, elements with X-ray peaks close to Fe, such as Mn may then be affected by the Fe peak. One the other

hand, the Mn peaks are isolated are not influenced by other elements within the alloy. Hence the present study will be based on data solely from the Mn peaks.

*2.3. Analysis tools*

The segregation ratio allows the comparison of segregation intensities, patterns or occurrence on different samples from different steel grades. For each chemical segregation map, the segregation ratio, $S_i$, for a specific element $i$ is calculated for each point of the map with the formula:

$$S_i = \frac{C_i - \bar{C}_i}{\bar{C}_i} \quad (1)$$

where $C_i$ is the local composition for the element $i$ and $\bar{C}_i$ the average composition on the map.

The use of a local segregation ratio, processed with the average composition from a single sample plate focuses the analysis on segregation at the sample scale. However, this methodology assumes that segregation between the sample plates is negligible. In the present study, this sample-based local segregation ratio is used, and thus, it is assumed that there is no macro or global segregation between the sample plates. Experimental data can be filtered to reduce small scale spatial variations. Different filters were tested to treat segregation maps obtained from µXRF measurements. Filters assign a new value to each point of the map. With a Gaussian filter, a weighted average is calculated using a Gaussian weighting function that depends on the distance between from the point, thus the close neighbourhood of the point has a greater influence on the weighted average than more distant areas.

## 3. Results and discussion

*3.1. Chemical segregation maps*

Thirty successive chemical segregation maps were collected with µXRF, giving access to 3D information on segregations. In Figure 2, two example maps are shown: the lowest in the ingot and another which was cut 5 mm above the first one. On both maps, the small acquisition step (100 µm) allows the observation of microsegregation with evident enrichment between secondary dendritic arms. In the bottom left quadrant of both maps, there are two strongly enriched regions. These regions exist on numerous successive plates and correspond to channel segregates which have been cut transversely. An example channel segregate transverse section is indicated in red on the maps in Figure 2. In the top right quadrant of Figure 2(a), enrichment is observed at a larger scale than microsegregation which is present between dendrite arms, but does not appear on the second map and is smaller than the channel segregation sections, as such this is another kind of segregation.

The present study aims at the reconstruction in 3D of the intermediate and large scale segregations. The first step is to eliminate the effect of microsegregation and highlight mesosegregations and channel segregates on each of the segregation maps.

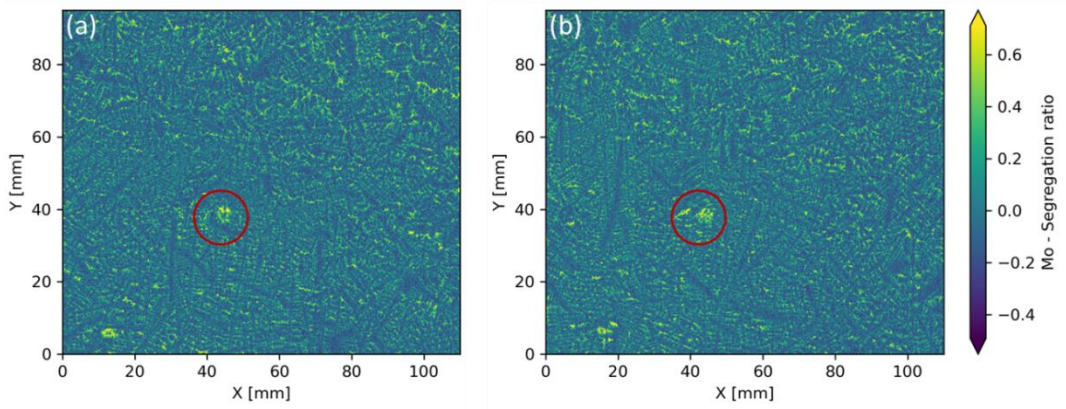


**Figure 2.** Mo segregation ratio maps of sample (a) N°1 and (b) N°2, the lowest and second lowest samples of the stack.

### *3.2. Filtration of raw chemical segregation maps*

Filters were used to eliminate microsegregation patterns from the segregations maps to study larger segregations patterns. As the filter influences the final map obtained, it is important to choose it appropriately, thus several filters were studied. In Figure 3, a map obtained from µ-XRF measurements and three filtered maps are presented. The filter used is a truncated Gaussian filter. The filtered segregation ratio $S_i^f$ is given by:

$$S_i^f(x_j, y_j) = \frac{1}{0.911}\int_{y_j-a/2}^{y_j+a/2}\int_{x_j-a/2}^{x_j+a/2}\frac{1}{2\pi\sigma^2}\exp\left(-\frac{(x-x_j)^2+(y-y_j)^2}{2\sigma^2}\right) S_i(x,y)\,dx\,dy \qquad (2)$$

The truncation of the Gaussian kernel is by a square with a side of $a = 4\sigma$, the coefficient 0.911 is obtained after integration of the truncated Gaussian kernel.Three different standard deviations of the kernel were tested: 13, 25, or 50 pixels, as one pixel is 100 µm the standard deviations tested are 0.13, 0.25 and 0.50 cm.

With a 0.13 cm standard deviation Gaussian kernel (Figure 3(b)), the segregation between dendritic arms is removed, however the depleted dendritic trunks are still visible. The second filter tested, with a 0.25 cm standard deviation Gaussian kernel, leads to a microsegregation free map on which channel segregates are clearly identifiable (Figure 3(c)). Finally, with the last filter tested the channel segregates shown in Figure 3(d) can no longer all be identified and the enrichment and depletion intensities were decreased to level below which useful information can be gathered.

The treatment of the successive segregation maps was then done using the selected 0.25 cm standard deviation Gaussian kernel to eliminate microsegregation from the maps while retaining useful information on the prioritized analysis of the channel segregates. The following 3D reconstruction is based on binary images obtained by the application of a suitable threshold to these filtered maps.

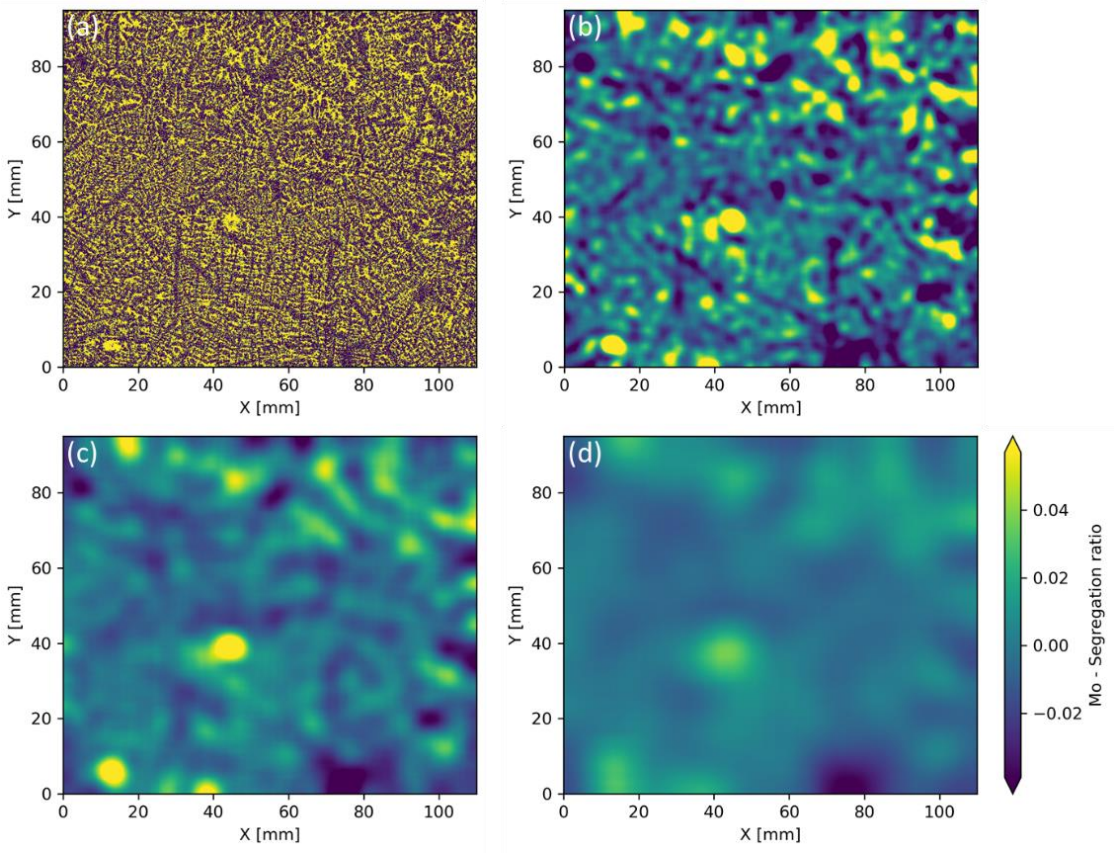


**Figure 3.** Mo segregation map from sample N°1 with different Gaussian filters applied. The truncation of the Gaussian kernel is 4$\sigma$ and 3 standard deviation values are presented ((a) unfiltered map, (b) $\sigma$ = 0.13 cm, (c) $\sigma$ = 0.25 cm, (b) $\sigma$ = 0.50 cm).

*3.3. 3D reconstruction and observation of segregations*

The filtered maps were binarized with a segregation ratio threshold of 0.029, i.e., any pixel with a segregation ratio superior to 0.029 was considered to be a part of the segregations to observe in 3D and kept in the map, whereas any value below was eliminated. This segregation ratio was fixed so the volume of segregations reconstructed in 3D corresponds to 5% of the total volume analysed. A higher threshold would reduce the reconstructed segregation patterns and it would not reveal continuous channel segregates. On the other hand, a lower threshold increases the number and size of 3D segregation patterns which hides the channel segregates in the images. In Figure 4, the segregation ratio map of the lowest sample is presented after filtration (Figure 4(a)) and after binarization using this threshold (Figure 4(b)). On the segregation map (Figure 4(a)), the red lines show the 0.029 segregation ratio threshold. After binarization, the segregation ratio map of sample N°1 turns to the image displayed in Figure 4(b). Each of the segregation maps from the sample plates were filtered and made binary, afterwards the free, open source software 3DSlicer [15] was used to reconstruct the segregation volume.

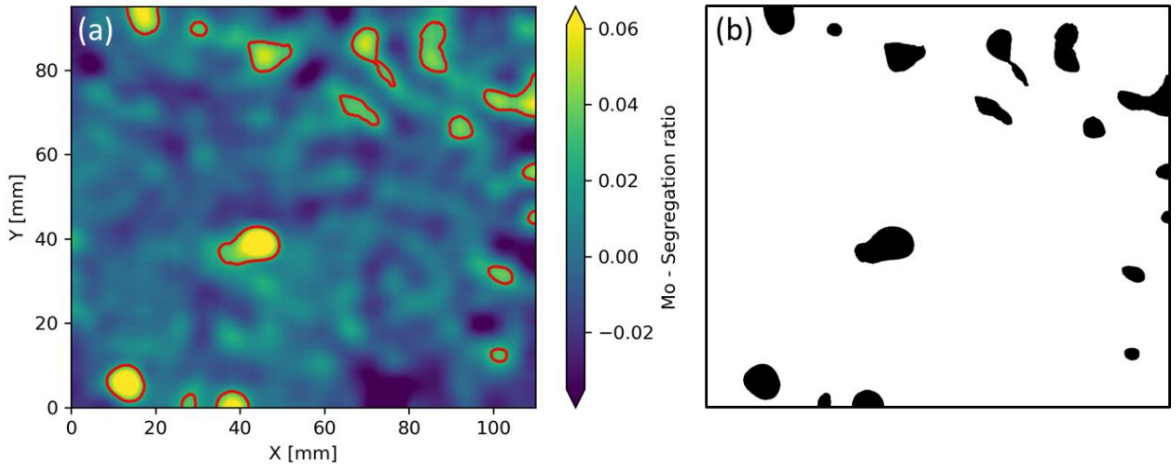


**Figure 4.** Binarization process for reconstruction, (a) the Gaussian-filtered chemical segregation map, with the segregation ratio threshold of 0.029 highlighted in red (b) the map obtained after binarization with this threshold.

The 3D reconstruction presented in Figure 5 was made by interpolation between each of the 30 binarized maps. The orientation of the reconstruction follows the previously defined co-ordinates also shown in Figure 1, i.e., the $x$-direction is the radius of the ingot and the $z$-direction is the height.

The 3D reconstruction shows different segregation patterns at different scales. Several channel segregates exist within the volume analysed, some go through the entire volume from bottom to top, appearing in each sample plate while others merge together or appear from within the volume. Other smaller segregations can be observed within the volume, appearing only on limited number of sample plates, without the classical shape of the observed channel segregates. These segregations are larger than microsegregation since they exist at a larger scale than the secondary dendritic arm spacing, however they are smaller than the channel segregates and cannot be linked to macrosegregation at the ingot scale. These smaller segregations observed in the volume are intermediate scale segregation. The characterisation of these segregates, such as their size, distribution, occurrence, or shape using such tools as geostatistical analysis remains a key task to better understand the occurrence of mesosegregation.

## 4. Conclusion

The observation of segregation in a 3D volume is key to understand their formation. The objective of this work was to analyze different segregation patterns in 3 dimensions at a centimetric scale. The analysis of serial cut samples with µXRF reveals segregations patterns at different scales. Image treatment techniques such as Gaussian filters were used to eliminate microsegregation patterns and

prioritize investigations on intermediate scale and channel shape segregation. The maps of these remaining segregations were then binarized with a segregation ratio threshold of 0.029 to clearly identify channel segregates on successive samples and enable their reconstruction in 3D. The volume representation of segregations shows the co-existence of several channel segregates with intermediate scale segregations, which cannot be identified as micro- or macrosegregation. These mesoscale segregations require a comprehensive study to quantify their size, shape, distribution and occurrence. This study can be based on the present experimental results, analyzed with geostatistics.

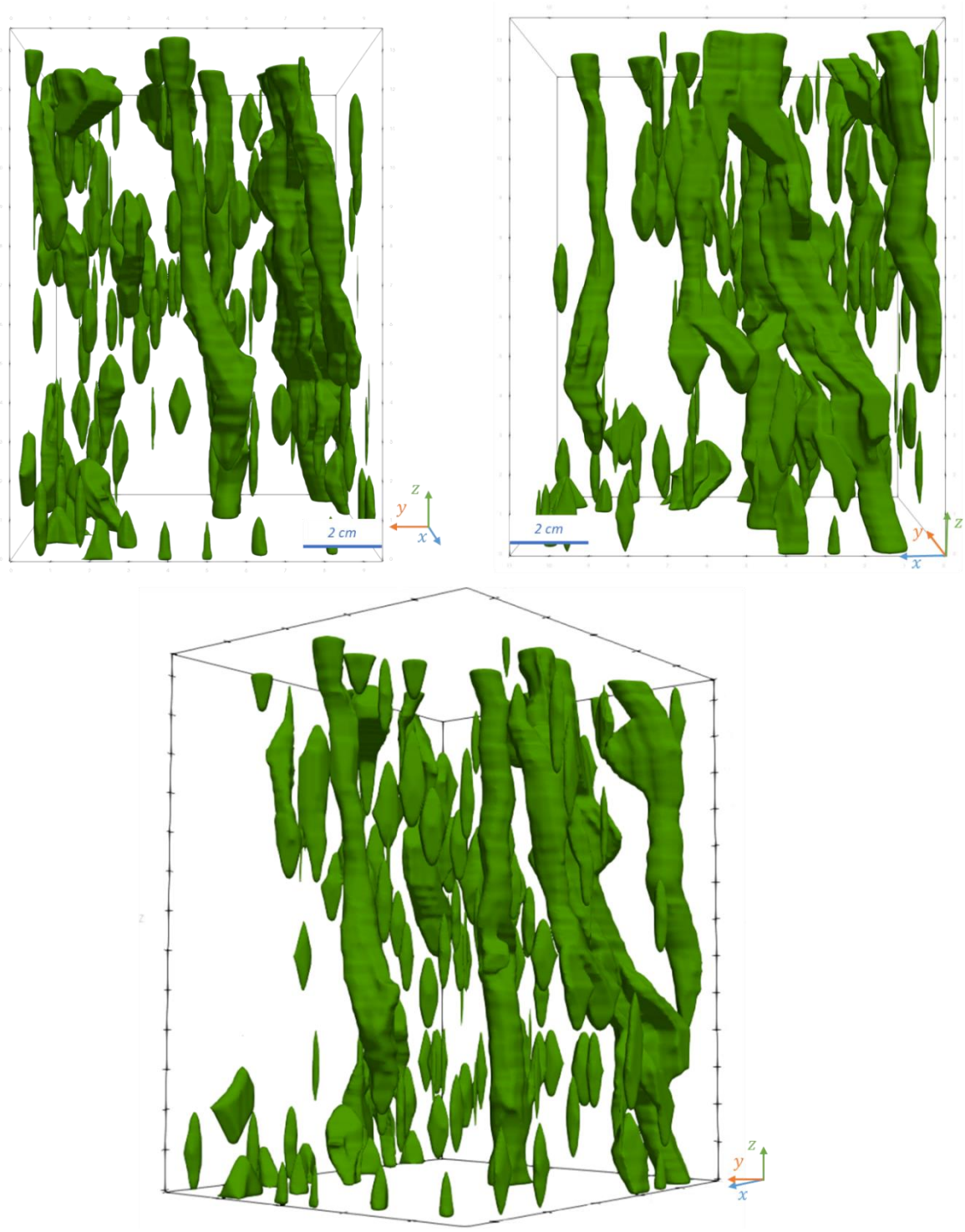


**Figure 5.** 3D reconstruction of sample volume showing channel and intermediate scale segregation.

**Acknowledgments**
This research work is supported by ANRT France under a CIFRE Ph.D. fellowship (Grant Number 2020/1234), through the Industrial chair Solidification at Institut Jean Lamour, supported by ArcelorMittal, ArcelorMittal Industeel, CEA, EDF and Framatome, and though µXRF usage provided by SCMEM at the Universite de Lorraine. A part of the required high performance computing resources was provided by the EXPLOR center hosted by the University of Lorraine.

**References**
[1] Lesoult G 1986 *Techniques de l'ingénieur. Matériaux métalliques.* **M58** 1
[2] Dantzig J A and Rappaz M 2009 *Solidification*. (Lausanne: EPFL Press) p 394
[3] Pickering E J 2013 *ISIJ international.* **53** 935–49
[4] Ludwig A, Wu M and Kharicha A 2015 *Metall. Mater. Trans. A* **46** 4854–67
[5] Thornthon P A and Colangelo V J 1976 *Metall. Mater. Trans. B.* **7** 425–33
[6] Pickering E J and Bhadeshia H K D H 2014 *J. Press. Vessel Technol. Trans. ASME.* **136**
[7] Salimi A, Zadeh H M, Toroghinejad M R, Asefi D and Ansaripour A 1996 *Materiali in tehnologije.* **47** 385
[8] Hong S, Song, J, Kim MC, Choi KJ and Lee BS 2015 *Met. Mater. Int.* **22** 196–203
[9] Yan, G *et al.* 2017 *Metallurgical and Materials Transactions A*. **48**, 3470-81.
[10] Vasileiou A N *et al*. 2021 *Materials and Design.* **209** 109924
[11] Yamashita T, Torizuka S and Nagai K 2003 *ISIJ international.* **43** 1833–41
[12] Pickering E J *et al*. 2015 *Metallurgical and Materials Transactions B.* **46** 1860–74
[13] Pickering E J and Holland M 2014 *Ironmaking & Steelmaking.* **41** 493–9
[14] Gutman L *et al*. 2023 *IOP Conf. Ser. : Mater. Sci. Eng.* **1274** 012049
[15] Fedorov A *et al*. 2012 *3D Slicer as an Image Computing Platform for the Quantitative Imaging Network. Magnetic Resonance Imaging.* 1323-41. PMID: 22770690. PMCID: PMC3466397.